Hindawi Publishing Corporation
Journal of Climatology
Volume 2014, Article ID 434960, 10 pages
http://dx.doi.org/10.1155/2014/434960

Research Article

On the Differences in the Intraseasonal Rainfall Variability between Western and Eastern Central Africa: Case of 10–25-Day Oscillations

Alain Tchakoutio Sandjon,[1,2] Armand Nzeukou,[1] Clément Tchawoua,[3] and Tengeleng Siddi[1,4]

[1] *Laboratory of Industrial Systems and Environmental Engineering, Fotso Victor Technology Institute, University of Dschang, Cameroon*
[2] *Laboratory for Environmental Modeling and Atmospheric Physics, Department of Physics, Faculty of Sciences, University of Yaoundé 1, P.O. Box 812, Yaoundé, Cameroon*
[3] *Laboratory of Mechanics, Department of Physics, Faculty of Science, University of Yaoundé 1, Cameroon*
[4] *Higher Institute of Sahel, University of Maroua, Cameroon*

Correspondence should be addressed to Alain Tchakoutio Sandjon; stchakoutio@yahoo.com

Received 29 January 2014; Accepted 31 March 2014; Published 23 April 2014

Academic Editor: Maxim Ogurtsov

In this paper, we analyze the space-time structures of the 10–25 day intraseasonal variability of rainfall over Central Africa (CA) using 1DD GPCP rainfall product for the period 1996–2009, with an emphasis on the comparison between the western Central Africa (WCA) and the eastern Central Africa (ECA) with different climate features. The results of Empirical Orthogonal Functions (EOFs) analysis have shown that the amount of variance explained by the leading EOFs is greater in ECA than WCA (40.6% and 48.1%, for WCA and ECA, resp.). For the two subregions, the power spectra of the principal components (PCs) peak around 15 days, indicating a biweekly signal. The lagged cross-correlations computed between WCA and ECA PCs time series showed that most of the WCA PCs lead ECA PCs time series with a time scale of 5–8 days. The variations of Intraseasonal Oscillations (ISO) activity are weak in WCA, when compared with ECA where the signal exhibits large annual and interannual variations. Globally, the correlation coefficients computed between ECA and WCA annual mean ISO power time series are weak, revealing that the processes driving the interannual modulation of ISO signal should be different in nature or magnitude in the two subregions.

1. Introduction

The monitoring and prediction of climate in the tropics remain a crucial problem in the scientific community. It is well-known that many regions in the tropics are vulnerable to climate change because their resources are highly rainfall dependent. Amongst these regions, Central Africa (CA) is particularly vulnerable because the majority of its population is rural and practice rain-fed agriculture [1]. A strong rainfall intensity can result in devastating floods, whereas a weak rainfall is usually associated with droughts, thus affecting living conditions and the economy of the densely populated region in many sectors such as agriculture, livestock, and energy [2, 3].

The CA extends from 15°S to 15°N and 0–50°E mainly over the land and part of Atlantic and Indian Oceans on its edges (Figure 1). The topography of the region is quite various, including highlands, mountains, and Plateaus. The western part (15°S–15°N; 0–30°E) is consisting of the zones of intense precipitation, especially over the Congo Basin [4]. Some of the highest rainfall totals are reported over Mountain Cameroon, at its western edge, where mean annual rainfall exceeds 10 meters. The Congo basin was proven to experience one of the world's most intense thunderstorms and highest frequency of lightning flashes [5, 6]. The western central Africa is almost covered by the Congo forest, which keep this region quite wet within the year. The Eastern part (15°S–15°N; 30–50°E) is characterized by widely diverse climates ranging

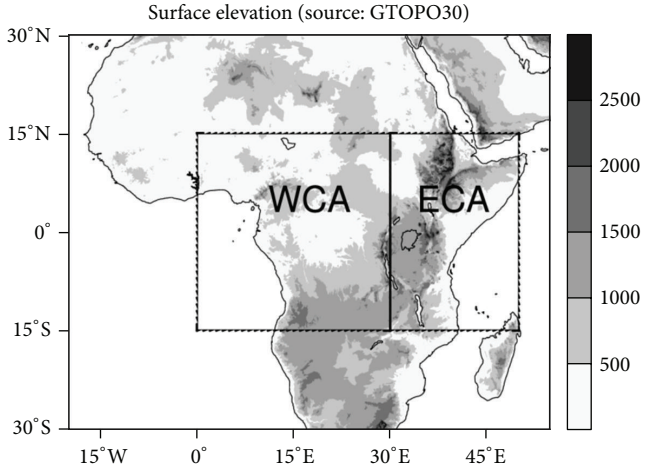

Figure 1: Surface elevation over the study area based on 30 min topographic data (m) from Digital Elevation Model (DEM) of the US Geological Survey. The study domain (15°S–15°N, 0–50°E) and the division line between WCA and ECA are shown on the plot.

Table 1: Comparison of some geographical features between ECA and WCA.

	Western Central Africa (west of Rift Valley)	Eastern Central Africa (east of Rift Valley)
Average topography	Lower than 700 m	Greater than 1500 m
Vegetation	Almost covered by the Congo forest	From desert to small forests over relatively small areas
Mean annual rainfall	Greater than 1600 mm	Lower than 700 mm
Borders	Rift Valley-Atlantic Ocean	Rift Valley-Indian Ocean

from desert to forest over relatively small areas. The complex topography of the region is an important contributing factor to climate because it leads to the orographically induced rainfall and affects local climates [7]. This region has suffered both excessive and deficient rainfall in recent years [8, 9]. In particular, the frequency of anomalously strong rainfall causing floods has increased. The difference between the east and west boundaries of CA is of approximately 3000 m in surface elevation and 3000 mm in annual mean rainfall. Then the two subregions (ECA and WCA), separated from each other by the Rift Valley, are very different in terms of topography, surface conditions, and precipitation (Table 1).

Rainfall variability in the tropics is complex, including different timescales ranging from few hours to a few months. Before the 1970s, the lack of high temporal resolution datasets leads many authors to the study of the rainfall fluctuations in the tropics in terms of annual cycle and interannual variability. The processes that induce rainfall variability within the season could not be investigated because it requires a high temporal resolution data. But since the beginning of the 1970s, the emergence of satellite data produced capability to estimate regional or global rainfall fields at higher resolution, from the satellite measurements. Therefore, the notion of intraseasonal variability (ISV) arose in the scientific community and many authors used different rainfall or rainfall proxy datasets to study ISV in the tropics [10, 11].

Some of these authors have studied the ISV in precipitation for different geographical regions of Africa. For example, significant spectral peaks around 15- and 40-day period were found for Sahel precipitation by [12]. Analysis was made for Africa and signals over 10–25- and 25–60-day period were found in convection and precipitation in the western region [12–14]. [15] using outgoing long-wave radiation data developed climatology for tropical intraseasonal convective anomalies. [16] investigated the influence of the Madden-Julian oscillation on East African rainfall and showed that MJO phases leading to wet spells in the eastern (coastal) region are often those associated with overall suppressed deep convection in the Africa/Indian Ocean region. [17] have investigated the spatial and temporal structure of intraseasonal oscillations over Central Africa using 21 years (1980–2000) of pentad (5 day) rainfall and low level wind and they found three dominant modes for intraseasonal rainfall with the period of around 40–50 days. [18] used principal components analysis and Satellite-Derived Rainfall data to show that major cycles of intraseasonal rainfall events over Southern Africa are around 20 and 40 days.

Our understanding of the climate processes in CA is limited. Indeed, the literature on African climate variability is strongly biased towards West Africa (including the Sahel), East Africa, and Southern Africa. Thus, the CA region represents a notable gap in the study of the tropical climate system. Significantly, the structure of the intraseasonal oscillations (ISO) in Central Africa is only discussed by few authors [4, 17, 19, 20]. More recently, [19] used one-Degree Daily Global Precipitation Climatology Project (1 DD GPCP) higher resolution rainfall product to study the ISO patterns in CA, but they considered the whole area (15°S–15°N, 0–50°N) and did not take into account the contrast patterns between western and eastern parts of the region with different climate features.

Reference [4] also considered the whole area, and they showed that the East African modes (Ethiopian and Tanzanian modes) exhibit strong interannual variations, when compared with West African mode (Congo mode). Then the major issue of this study is the comparison of intraseasonal oscillations (ISO) patterns between western Central Africa (WCA) and eastern Central Africa (ECA). From the difference between physical features of ECA and WCA, one central question we may ask is "*what could be the difference in the ISO patterns between WCA and ECA?*" Some of the previous studies revealed two dominant frequency bands (10–25 and 25–60 days) at the intraseasonal timescale in tropical Africa [12–14], but for this study, we focused on the case of 10–25-day band. We use simple mathematical tools to assess the detailed spatial and temporal patterns of the leading modes of ISV of rainfall over the region, both throughout the year and from year to another.

In the next section, the data and method of analysis will be described. Section 3 will present the main results obtained

and their analysis. Finally, Section 4 is devoted to a few discussions and conclusions.

2. Data and Methods

For this study, we used the 1DD GPCP rainfall data. The GPCP algorithm combines precipitation estimates from several sources, including infrared (IR) and passive microwave (PM) rain estimates and rain gauge observations [22, 23]. The IR data came mainly from the different Geostationary Meteorological Satellites but data from polar-orbiting satellites were also used to fill in the gaps at higher latitudes. The IR based estimates used the Geostationary Operational Environmental Satellite (GOES) precipitation index (GPI) described by [24]. The microwave data come mainly from the Special Sensor Microwave Imager (SSM/I) onboard the Defense Meteorological Satellite Program. The PM estimates were used to adjust the GPI estimate. Then, the multisatellite estimate was adjusted towards the large-scale gauge average for each grid box. The gauge-adjusted multisatellite estimates were then combined with gauge analysis using a weighted average, where the weights are the inverse error variances of the respective estimates. The current products include a monthly analysis at $2.5^\circ \times 2.5^\circ$ longitude-latitude grids, a 5-day (pentad) analysis at the same spatial resolution, and a daily product at a special resolution of one degree. The one-degree daily (1DD) product does not use PM rain estimates and gauge measurements directly [22]. SSM/I data were used within the framework of the threshold-matched precipitation index (TMPI) to delineate rain areas in the IR data. Gauge data were involved indirectly when the 1DD product was scaled so that monthly accumulations of 1DD matched the monthly GPCP product. The monthly and pentad analyses extend from 1979 to current, while the daily product is available starting from October 1996. The daily products are made available 2 to 3 months after the end of each month. The product used in this paper is the one-degree daily precipitation data available on the NOAA website http://www.esrl.noaa.gov/psd/data/gridded/data.gpcp.html. After some global and regional validations [25–27], the GPCP rainfall estimates are actually being used widely in place of gauge observations or to supplement gauge observations in the climate variability studies.

In the atmospheric sciences, climate is affected by the many phenomena with different spatial and temporal scales. To study the climate variability within a given scale, we generally use a digital filter to extract only the desired frequencies in a data time series. The Lanczos filtering [28, 29] used in this study is one of Fourier methods of filtering digital data. Its principal feature is the reduction of the amplitudes of Gibbs oscillation. Fourier coefficients for the smoothed response function are determined by multiplying the original weight function by a function that Lanczos called "sigma factors" (1):

$$\overline{w}_k = \frac{\sin 2\pi k f_c}{\pi k} \cdot \frac{\sin \pi k/n}{\pi k/n}, \quad (1)$$

where the first fraction is the original weight function and the second is Lanczos factor.

The wavelet analysis (WA) is a time series analysis method that has increasingly been applied in geophysics during the last three decades. It is becoming a common tool for analyzing temporal variations of power within a time series. The transformation in time series from the time space into the time-frequency space show that the WA is able to determine both the dominant timescales of variability and how they vary with time. WA has several attractive advantages over the traditional Fourier analysis, especially when dealing with time series with time-varying amplitudes. In contrast, to Fourier transform, that generate values of amplitudes and phases averaged over the entire time series for each frequency component or harmonic, wavelet transform provide a localized instantaneous estimate of the amplitude and phase for each spectral component of the series. This gives WA an advantage in the analysis of nonstationary data in which the amplitude and phase of the harmonic components may change rapidly in time or space. While Fourier transform of the nonstationary time series would smear out any detailed information on the changing features, the WA keeps track of the evolution of the signal characteristics throughout the time. Further details on wavelet analysis can be found in [30].

Empirical Orthogonal Functions (EOF) analysis is a powerful tool for identifying coherent patterns that explains the largest fraction of the total variance of a field and it has been used extensively in studies of intraseasonal variations in tropical convection [31–33]. The EOF analysis is used in this study to define space-time structures of the dominant modes of intraseasonal variability in our study area. In the EOF analysis, the time-dependent deviations from the long-term mean are decomposed into a sum of products of fixed spatial patterns p_k and time-dependent amplitudes α_k (the principal components) as follows:

$$f(x_i, t) = \sum p_k(x_i)\,\alpha_k(t). \quad (2)$$

In (2), the principal components, α_k, are uncorrelated to one another and described subsequently a maximum of variance in the original anomalies field, f. Under these conditions, EOFs, p_k are eigenvectors of the covariance matrix of f.

3. Results and Analysis

3.1. Spectral Analysis. For every day, we averaged the data of all grid points in each of the two subregions (WCA and ECA) of the study area to have a mean value. The spectral analysis was then performed separately on the two daily area mean time series obtained. In Fourier decomposition, the importance of a given frequency in a time series can be quantified by the spectral variance, defined as the amplitude of the harmonic corresponding to the this frequency. The power spectra in the two subregions reveal the importance of the intraseasonal variability in Central African climate (Figure 2). However, one should note that the dominance is less pronounced in WCA when many significant peaks are observed at different frequencies in synoptic scale. The fraction of total variance occurring in the 35- to 80-day range is 0.33 for WCA and 0.48 for ECA. Wavelet analysis clearly revealed that the processes inducing rainfall variability

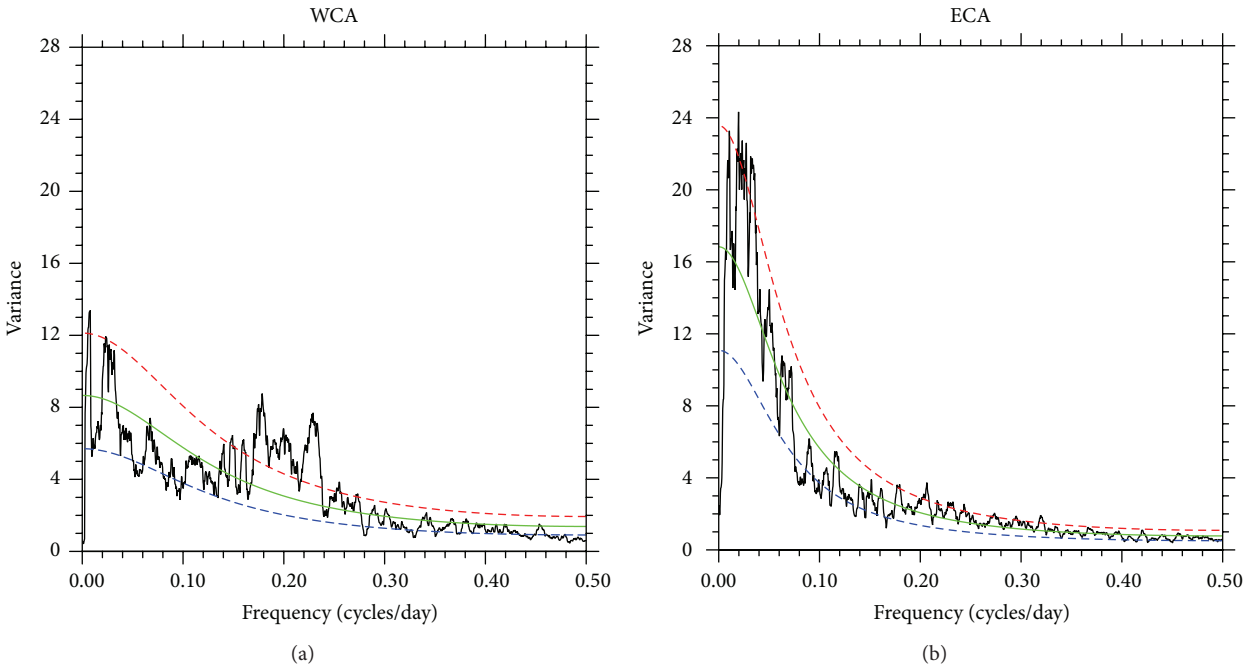

FIGURE 2: Calculated spectrum (solid black), red noise curve (green solid), and the curves indicating the upper (red dashed) and lower (blue dashed) bounds of 95% confidence level, for WCA (a) and ECA (b) subregions. The red noise spectrum is computed using the Markov processes [21].

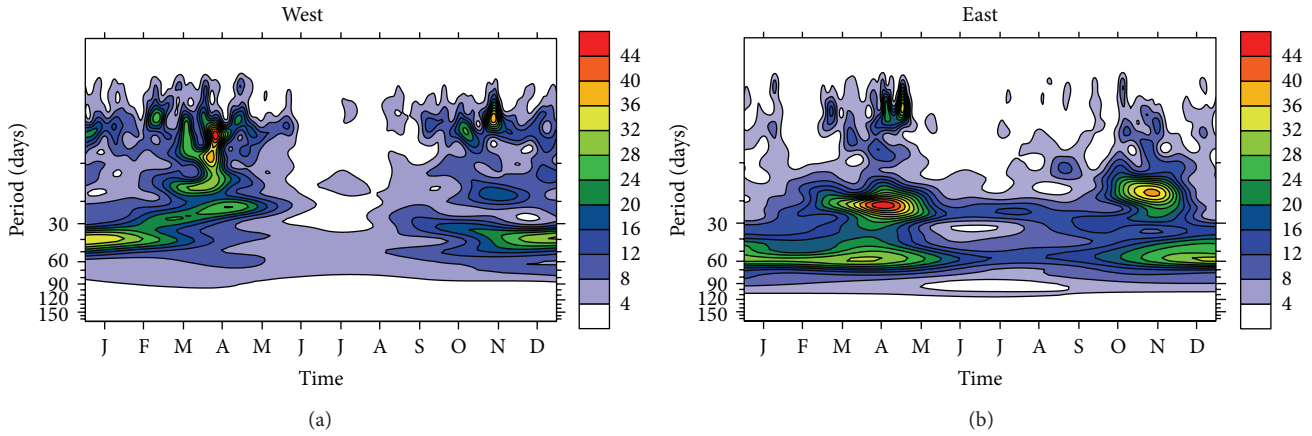

FIGURE 3: Annual mean wavelet power of the rainfall anomalies averaged over WCA (a) and ECA (b). A 120-day cutoff high pass filter was applied to long term anomalies in order to remove low frequencies variability such as interseasonal and interannual variability.

in the CA vary from synoptic (below 10 days) to longer timescales (Figures 3(a) and 3(b)). From the spectra, it is easy to identify the two bands of high wavelet powers in the ECA spectrum (10–25 days and 25–70 days), while in the WCA the relative importance of synoptic scale (below 10 days) does not allow to easily highlight the two intraseasonal periods bands. This shows that in WCA, the mechanisms that induce are much rainfall varied. At the synoptic scale, the spectral power peaks near 5 days in the two subregions. Nevertheless, the signal is predominantly contained within 10 and 70 days with two dominant timescales (10–25 days and 25–70 days), much highlighted in the ECA spectrum (Figure 3(b)). This result is consistent to that found by other authors [14, 34] with daily OLR datasets over West Africa. The seasonality of wavelet power is clearly defined, showing the maximum power during the beginning and end of the year. In fact, this seasonality can be explained by the location of study area along the equator [35]. The peak of ITCZ precipitation belt shifts from north to south of the equator during November-December and returns to north during March-April.

3.2. Intraseasonal Oscillations. The spectral analysis performed above leads us to filter the rainfall anomalies either between 10 and 25 days to derive the space-time structures

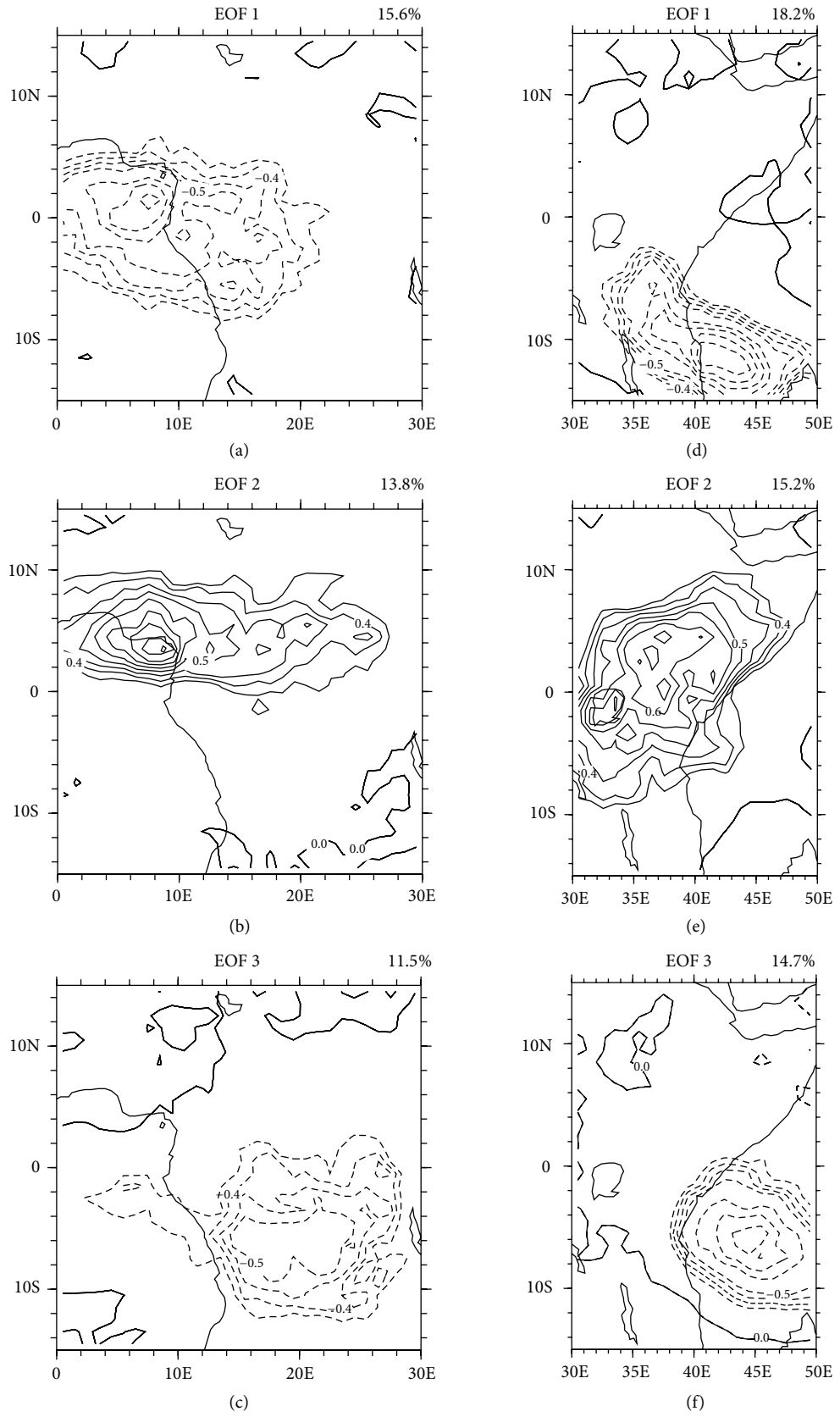

Figure 4: Correlation coefficient map (loadings) between rainfall anomalies field and PCs for WCA (a, b, c) and ECA (d, e, f). PCs were computed using the whole time series of daily rainfall for the period 1996–2009. Contour intervals are plotted every 0.05 and correlations in between −0.2 and 0.2 are omitted. The negative correlations are represented as dashed line and the positive correlation the solid lines.

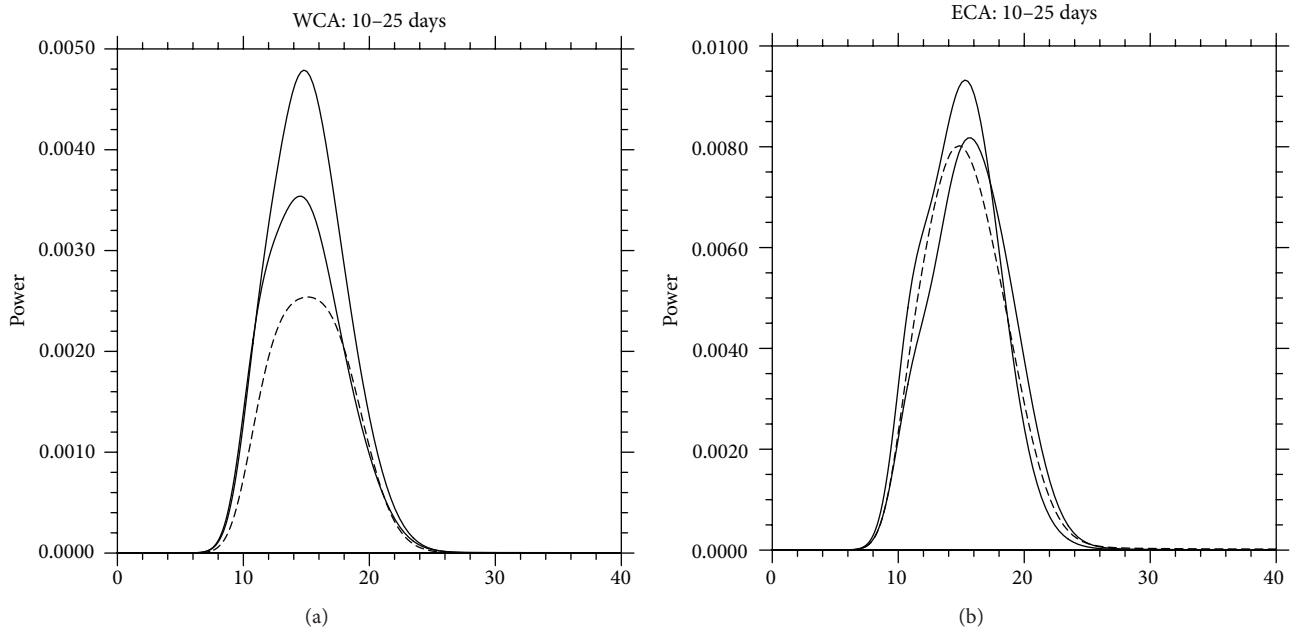

Figure 5: Power spectra of PC1 (Bold solid), PC2 (thin solid), and PC3 (thin dashed), respectively, over WCA (left top and left bottom) and ECA (right top and right bottom). The scale of the x-axis is in days for all plots and the power dimensionless because the anomalies field is normalized.

of the leading EOFs of 10–25-day intraseasonal variability of rainfall over CA. All these analyses are performed separately in ECA and WCA. The leading modes are retained according to the Scree test [36] and the North criteria [37], and spatial loadings associated with a given mode are obtained by computing the correlation coefficients between the corresponding PC's time series and the filtered data field.

The leading eigenvector and the next two are accounting for, respectively, 15.8%, 13.8%, and 11.3% of the variance for WCA and 18.2%, 15.2%, and 14.7% for ECA (Figure 4). For WCA, all three leading EOFs have positive loadings (Figures 4(a)–4(c)). The first two modes are centered over the Atlantic Ocean near the equator and extend to cover a part of the land and the Atlantic Ocean, while the third is centered over the land and extends over the Congo Forest. Over ECA, the spatial loadings of first and third EOFs are negative, while the second is positive (Figures 4(d)–4(f)). The amount of the total variance explained by the leadings EOFs is smaller in WCA (40.6%) than ECA (48.1%), suggesting that rainfall time series in WCA have more degree of freedom. These results are consistent with the spectral analysis of Section 3.1.

The power spectra of the three principal components (PCs) peak around 15 days both in WCA and ECA (Figure 5). The amplitude time series reveals a difference between ECA and WCA 10–25-day rainfall oscillations. WCA experiences intraseasonal oscillations (ISO) almost throughout the year and the contrast between the seasons is less pronounced, but there are relative bursts of signal amplitude during the October–April season (Figures 6(a)–6(c)). However, the seasonality of oscillations is well defined in ECA (Figures 6(d)–6(f)), as the oscillation amplitudes maximize during October–April and there are weakened or no oscillation during the rest of the year.

It is well known that the slow eastward propagation at an average speed of 5 m·s^{-1} [31] is one of the most fundamental features that distinguishes the MJO from other phenomena in the tropical atmosphere, especially, convectively coupled Kelvin waves, which propagate eastward at greater speeds of 15–17 m s^{-1}. This eastward propagation could potentially be the relationship between WCA and ECA modes of intraseasonal variability. In Figure 7, the lagged correlations are displayed between the WCA and ECA PCs time series. This figure clearly reveals that the observed PC's time series exhibit a characteristic lead/lag structure. The relatively high maximum positive correlation indicates that most of the WCA PC's lead ECA PCs time series with a time scale of 5–8 days. This result suggests a zonal propagation of EOF modes found above. Averaging filtered data between 15°N and 15°S, and plotting lagged correlation as a function of longitude, succinctly captures ISO propagation (Figure 8). Regression of the ISO indices [4], with filtered GPCP and 850 hPa zonal wind, are performed using the data over Central Africa (15°N–15°S; 0–50°E).

The eastward propagation of the ISO is associated with low-level convergence. The 850 hPa convergence anomalies lead the convection, showing enhanced easterlies (westerlies) ahead (behind) enhanced rainfall as the ISO propagates through the global tropics. The average duration of an intraseasonal event to move from 0 to 45°E is approximately 7 days.

3.3. Interannual Variations in the ISO Amplitude. In the previous section, it was shown that the ISO amplitude exhibits

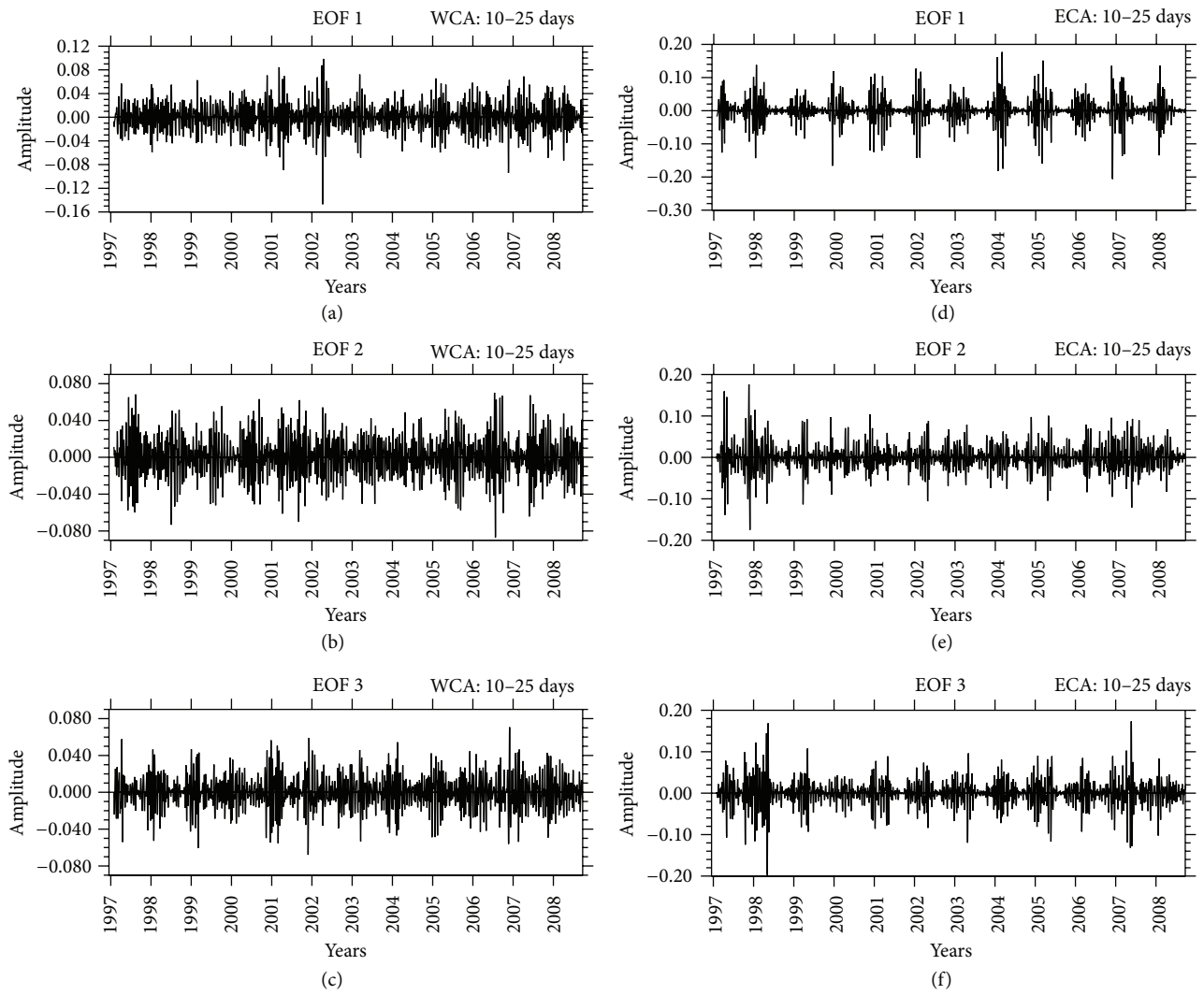

Figure 6: Principal components (scores) time series of the 10–25-day filtered rainfall anomalies for WCA ((a)–(c)) and ECA ((d)–(f)).

large interannual variations in ECA, when compared with WCA. Moreover, it was proved by many previous studies that an important characteristic of the MJO (ISO) is its irregularity from year to another [4, 38, 39]. Figure 9 shows the interannual variations in the ISO power over WCA (Figure 9(a)) and ECA (Figure 9(b)). For every year, the ISO strength is accessed by taking the mean squared amplitude of each PCs time series. The interannual variations of ISO strength are coherent for all the three PCs in each of the two subregions, as can be seen by the high values of the correlation coefficients (Table 2). But the correlation coefficients computed between the WCA and ECA ISO power time series are relatively low (Table 3), showing that the processes driving the interannual modulation of ISO signal are different in nature or magnitude in the two subregions. It can also be seen that the ISO strength experienced the highest fluctuations during the end of the 1990s and the beginning of the 2000s. For the two subregions, the variations of ISO activity during the end of the 1990s and early 2000s are similar. This period is marked by above normal ISO activity in the year 1997, followed by the below normal ISO activity during 1997–2001. The difference clearly appears toward the end of the study period. For the two timescales, ECA is characterized by below normal ISO activity during the years 2005–2008, while during the same period, the WCA experienced above normal ISO activity in many years. Further investigations are required to identify the causation of the coherent interannual variations of ISO signal during this period.

4. Summary and Conclusions

ISV of rainfall over Central Africa was examined using 1DD GPCP rainfall product for the period 1996–2009, with an emphasis on the comparison between western Central Africa (WCA) and eastern Central Africa (ECA), with different climate features. The classical Fourier analysis revealed the importance of ISV in Central African climate, but the dominance of intraseasonal band is more highlighted in ECA,

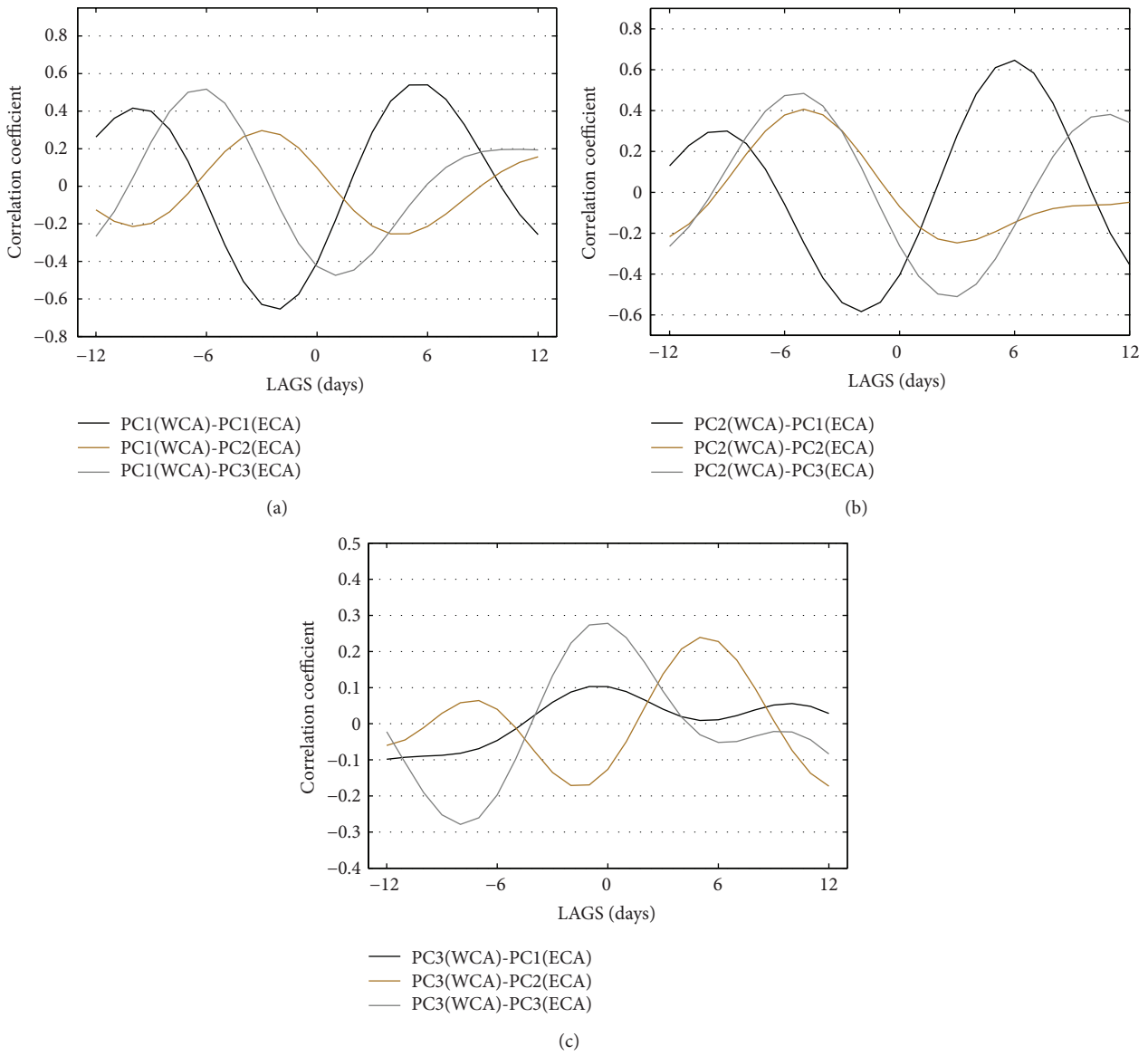

Figure 7: Lead-lag correlation between ECA and WCA 10–25-day PC's time series. Positive correlations at positive time lags indicate that convection over WCA leads that over the ECA.

Table 2: Correlation coefficients between WCA and ECA annual mean ISO power.

	WCA	ECA
PC1-PC2	0.43	0.51
PC1–PC3	0.61	0.12
PC2-PC3	0.73	0.47

Table 3: Cross-correlation coefficients between WCA and ECA annual mean ISO power.

WCA	ECA		
	PC1	PC2	PC3
PC1	−0.09	0.06	−0.05
PC2	−0.12	0.15	0.13
PC3	0.1	−0.11	−0.01

when compared with WCA. A wavelet analysis showed that intraseasonal precipitation variability in CA is dominated by two distinct timescales (10–25 days and 25–70 days) with significant spectral peaks centered, respectively, around periods of 15 days and 50 days, in consistency with the classical Fourier analysis. The seasonality of the ISO power is evident, showing the maximum power at the beginning and end of the year. But this seasonality is well defined in ECA, unlike WCA where the signal persists almost throughout the year.

For 10–25-day band, the result of EOF analysis of the filtered data has shown that the leading eigenvectors vectors explain about 40.6% of total intraseasonal rainfall variability

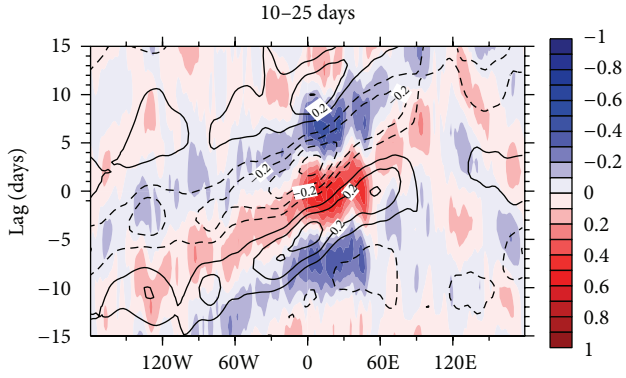

Figure 8: ISO composite based on the correlation between bandpass (10–25 days) filtered 850-hPa zonal wind (contours) and precipitation (colors) upon ISO index time series. The reference time series is Central Africa precipitation time series. The ISO index was computed using the average wavelet power.

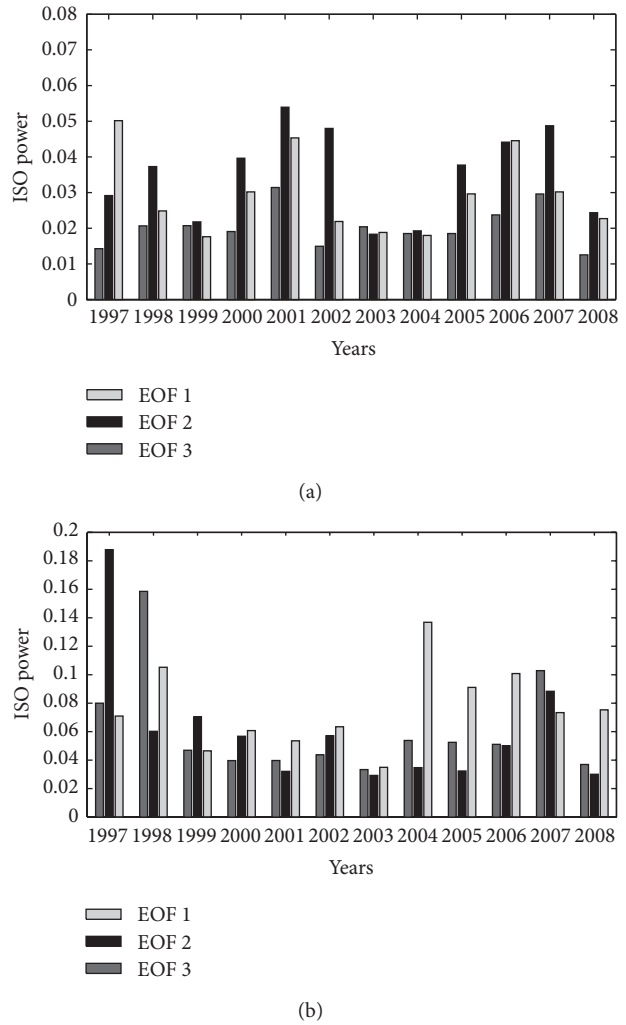

Figure 9: Interannual variations of ISO indices in WCA (a) and ECA (b), within the period 1997–2008, and for the three EOFs retained.

for WCA and 48.1% for ECA, suggesting that filtered rainfall time series in WCA have more degree of freedom than ECA. The spatial loadings are coherent, showing either positive or negative correlation coefficient between each eigenvector and rainfall. The power spectra of PCs peak around 15 days both in WCA and ECA.

The amplitude time series confirmed that rainfall variability in ECA is highly seasonal, revealing significant oscillations (wet/dry spells) with greater amplitudes during the beginning and end of the year (October–April) and weakened or no oscillation during the rest of the year. Once again, this seasonality is less pronounced in WCA PC's time series, but nevertheless the ISO amplitudes are relatively higher during October–April than other months.

An ISO strength index was built by averaging the wavelet power corresponding to each PC and for the 10–25-day timescales to form a daily indices time series. The plots of interannual variations of ISO strength clearly show that the signal over ECA exhibits larger interannual variations than WCA. Further investigations are needed to explain the causation of these patterns found.

The picture that emerges from these results is that the 10–25-day intraseasonal rainfall variability detected in 1DD GPCP rainfall shows some different patterns in ECA and WCA. The main difference between WCA and ECA modes is the variations of ISO strength. The variations in WCA are weak, compared to ECA where the signal exhibits large annual and interannual variations.

Conflict of Interests

The authors declare no conflict of interests.

Acknowledgments

Most of the scripts used in this study were produced from the NCL website http://www.ncl.ucar.edu/. The GPCP data was obtained from the NOAA website, http://www.esrl.noaa.gov/. All the administrator members of these websites are gratefully acknowledged for maintaining the updated data. The authors also thank the senior researchers of LEMAP and LISIE for helpful comments.

References

[1] UNEP DEWA/PAN-AFRICAN START, "Vulnerability of water resources to environmental change in Africa," River Basin Approach, UNEP, 2004.

[2] T. James and P. Karl, "Economic losses and poverty effects of droughts and floods in Malawi," OER Africa, 2009.

[3] P. Dierk, M. Charles, and H. Stefan, "Diagnosing the droughts and floods in equatorial east Africa during boreal autumn 2005–08," *Journal of Climate*, vol. 23, no. 3, pp. 813–817, 2010.

[4] A. S. Tchakoutio, A. Nzeukou, and C. Tchawoua, "Intraseasonal atmospheric variability and its interannual modulation in Central Africa," *Meteorology and Atmospheric Physics*, vol. 117, no. 3-4, pp. 167–179, 2012.

[5] E. J. Zipser, D. J. Cecil, C. Liu, S. W. Nesbitt, and D. P. Yorty, "Where are the most intense thunderstorms on earth?" *Bulletin*

of the American Meteorological Society, vol. 87, no. 8, pp. 1057–1071, 2006.

[6] G. Hong and G. Heygster, "Intense tropical thunderstorms detected by the special sensor microwave imager/sounder," *IEEE Transactions on Geoscience and Remote Sensing*, vol. 46, no. 4, pp. 996–1005, 2008.

[7] M. Thomas, C. H. C. John, G. Alexander, and J. C. Nicolas, "Temporal precipitation variability versus altitude on a tropical high mountain: observations and mesoscale atmospheric modelling," *Quarterly Journal of the Royal Meteorological Society*, vol. 135, no. 643, pp. 1439–1455, 2009.

[8] A. M. Moore, J. P. Loschnigg, P. J. Webster, and R. R. Leben, "Coupled ocean-atmosphere dynamics in the Indian Ocean during 1997-98," *Nature*, vol. 401, no. 6751, pp. 356–360, 1999.

[9] C. Mutai, S. Hastenrath, and D. Polzin, "Diagnosing the 2005 drought in equatorial East Africa," *Journal of Climate*, vol. 20, no. 18, pp. 4628–4637, 2007.

[10] R. A. Madden and P. R. Julian, "Description of global-scale circulation cells in the tropics with a 40–50 day period," *Journal of the Atmospheric Sciences*, vol. 29, pp. 1109–1123, 1972.

[11] T. Yamagata and Y. Hayachi, "A simple diagnostic model for the 30–50 days oscillation in the tropics," *Journal of the Meteorological Society of Japan*, vol. 62, no. 5, pp. 709–717, 1984.

[12] B. Sultan and S. Janicot, "Intra-seasonal modulation of convection in the West African monsoon," *Geophysical Research Letters*, vol. 28, no. 3, pp. 523–526, 2001.

[13] B. Sultan and S. Janicot, "The West African monsoon dynamics—part II: the pre-onset and onset of the summer monsoon," *Journal of Climate*, vol. 16, pp. 3407–3427, 2003.

[14] S. Janicot and F. Mounier, "Evidence of two independent modes of convection at intraseasonal timescale in the West African summer monsoon," *Geophysical Research Letters*, vol. 31, no. 16, Article ID L16116, 2004.

[15] R. W. Higgins, D. E. Waliser, J.-K. E. Schemm, C. Jones, and L. M. V. Carvalho, "Climatology of tropical intraseasonal convective anomalies: 1979–2002," *Journal of Climate*, vol. 17, no. 3, pp. 523–539, 2004.

[16] P. Camberlin and P. Benjamin, "Influence of the Madden-Julian oscillation on East African rainfall—I: intraseasonal variability and regional dependency," *Quarterly Journal of the Royal Meteorological Society*, vol. 132, no. 621, pp. 2521–2539, 2006.

[17] L. Tazalika and M. R. Jury, "Intra-seasonal rainfall oscillations over central Africa: space-time character and evolution," *Theoretical and Applied Climatology*, vol. 94, no. 1-2, pp. 67–80, 2008.

[18] M. R. Jury and C. Hector, "Intraseasonal variability of satellite-derived rainfall and vegetation over Southern Africa," *Earth Interactions*, vol. 14, no. 3, pp. 1–26, 2010.

[19] A. S. Tchakoutio, A. Nzeukou, C. Tchawoua, F. M. Kamga, and D. Vondou, "A comparative analysis of intraseasonal variability in OLR and 1DD GPCP data over central Africa," *Theoretical and Applied Climatology*, vol. 116, no. 1-2, pp. 37–49, 2014.

[20] A. S. Tchakoutio, A. Nzeukou, C. Tchawoua, B. Sonfack, and T. Siddi, "Comparing the patterns of 20–70 days intraseasonal oscillations over Central Africa during the last three decades," *Theoretical and Applied Climatology*, 2013.

[21] D. L. Gilman, F. J. Fuglister, and J. M. Mitchell, "On the power spectrum of 'red noise'," *Journal of the Atmospheric Sciences*, vol. 20, no. 2, pp. 182–184, 1963.

[22] G. J. Huffman, M. Morrissey, D. Bolvin et al., "Global precipitation at one degree daily resolution from multisatellite observations," *Journal of Hydrometeorology*, vol. 2, pp. 36–50, 2001.

[23] R. F. Adler, "The version-2 Global Precipitation Climatology Project (GPCP) monthly precipitation analysis (1979-present)," *Journal of Hydrometeorology*, vol. 4, pp. 1147–1167, 2003.

[24] P. A. Arkin and B. N. Meisner, "The relationship between large-scale convective rainfall and cold cloud over the Western Hemisphere during 1982–84," *Monthly Weather Review*, vol. 115, no. 1, pp. 51–74, 1987.

[25] J. McCollum, E. Nelkin, D. Klotter et al., "Validation of TRMM and other rainfall estimates with a high-density gauge dataset for West Africa—part I: validation of GPCC rainfall product and pre-TRMM satellite and blended products," *Journal of Applied Meteorology*, vol. 42, no. 10, pp. 1337–1354, 2003.

[26] T. Dinku, P. Ceccato, E. Grover-Kopec, M. Lemma, S. J. Connor, and C. F. Ropelewski, "Validation of satellite rainfall products over East Africa's complex topography," *International Journal of Remote Sensing*, vol. 28, no. 7, pp. 1503–1526, 2007.

[27] F. Ruiz, T. Dinku, S. J. Connor, and P. Ceccato, "Validation and intercomparison of satellite rainfall estimates over Colombia," *Journal of Applied Meteorology and Climatology*, vol. 49, no. 5, pp. 1004–1014, 2010.

[28] C. Lanczos, *Applied Analysis*, Prentice-Hall, 1956.

[29] C. E. Duchon, "Lanczos filtering in one and two dimensions," *Journal of Applied Meteorology*, vol. 18, no. 8, pp. 1016–1022, 1979.

[30] C. Torrence and G. P. Compo, "A practical guide to wavelet analysis," *Bulletin of the American Meteorological Society*, vol. 79, no. 1, pp. 61–78, 1998.

[31] K. M. Weickmann and T. R. Knuston, "30–60 day atmospheric oscillations: composite life cycle of convection and circulation anomalies," *Monthly Weather Review*, vol. 115, no. 7, pp. 1407–1436, 1987.

[32] H. H. Harry and Z. Chindong, "Propagating and standing components of the intraseasonal oscillation in tropical convection," *Journal of the Atmospheric Sciences*, vol. 54, pp. 741–751, 1996.

[33] A. J. Matthews, "Intraseasonal variability over tropical Africa during northern summer," *Journal of Climate*, vol. 17, no. 12, pp. 2427–2440, 2004.

[34] E. D. Maloney and S. Jeffrey, "Intraseasonal variability of the West African monsoon and Atlantic ITCZ," *Journal of Climate*, vol. 21, no. 12, pp. 2898–2918, 2008.

[35] H. Rui and B. Wang, "Development characteristics and dynamic structure of tropical intraseasonal convection anomalies," *Journal of the Atmospheric Sciences*, vol. 47, no. 3, pp. 357–379, 1990.

[36] R. B. Cattell, "The scree test for the number of factors," *Multivariate Behavioral Research*, vol. 1, no. 2, pp. 245–276, 1966.

[37] G. R. North, T. L. Bell, R. F. Cahalan, and F. J. Moeng, "Sampling errors in the estimation of empirical orthogonal functions," *Monthly Weather Review*, vol. 110, no. 7, pp. 699–6706, 1982.

[38] H. H. Hendon, C. Zhang, and J. D. Glick, "Interannual variation of the Madden-Julian oscillation during austral summer," *Journal of Climate*, vol. 12, no. 8, pp. 2538–2550, 1999.

[39] J. M. Slingo, D. P. Rowell, K. R. Sperber, and F. Nortley, "On the predictability of the interannual behaviour of the Madden-Julian oscillation and its relationship with El Niño," *Quarterly Journal of the Royal Meteorological Society*, vol. 125, no. 554, pp. 583–609, 1999.